SPE 36651

Reservoir Fracture Mapping using Microearthquakes: Austin Chalk, Giddings Field, TX and 76 Field, Clinton Co., KY.

W.S. Phillips, J.T. Rutledge, SPE, and T.D. Fairbanks, Nambe Geophysical Inc, T.L. Gardner SPE and M.E. Miller, Exxon USA and B.K. Schuessler, Los Alamos National Laboratory

Abstract

Patterns of microearthquakes detected downhole defined fracture orientation and extent in the Austin chalk, Giddings field, TX and the 76 field, Clinton Co., KY. We collected over 480 and 770 microearthquakes during hydraulic stimulation at two sites in the Austin chalk, and over 3200 during primary production in Clinton Co. Data were of high enough quality that 20%, 31% and 53% of the events could be located, respectively. Reflected waves constrained microearthquakes to the stimulated depths at the base of the Austin chalk. In plan view, microearthquakes defined elongate fracture zones extending from the stimulation wells parallel to the regional fracture trend. However, widths of the stimulated zones differed by a factor of five between the two Austin chalk sites, indicating a large difference in the population of ancillary fractures. Post-stimulation production was much higher from the wider zone. At Clinton Co., microearthquakes defined low-angle, reverse-fault fracture zones above and below a producing zone. Associations with depleted production intervals indicated the mapped fractures had been previously drained. Drilling showed that the fractures currently contain brine. The seismic behavior was consistent with poroelastic models that predicted slight increases in compressive stress above and below the drained volume.

Introduction

Microearthquakes often accompany reservoir stimulation and production. By collecting high-quality seismic data, the microearthquakes can be mapped, yielding potentially extensive and high-resolution information about the fracture system. Fracture maps can be used to plan infill and horizontal drilling, and to design and evaluate hydraulic stimulation and enhanced recovery, production operations in fracture-dominated oil and gas reservoirs.

Borehole geophones at reservoir depths provide the high-quality data needed to determine microearthquake location patterns. But when special observation wells must be drilled, microseismic studies can be expensive. To demonstrate that high-quality data can be collected inexpensively, we deployed geophones in existing wells and developed techniques for analyzing data from the resulting, sparse array of instruments. We hope the demonstration of inexpensive and effective methods will result in the routine application of microearthquake techniques to study reservoir fracture systems.

Methods currently applied to study fracture systems include tilt-meter surveys that give gross fracture characteristics[1], and borehole optical, acoustic or resistivity (formation microscanner) surveys that give detailed information along the borehole[2]. More specialized methods include shear shadowing[3-6], coring or mineback experiments[7,8] and anisotropy from surface seismics[9]. While less detailed than borehole surveys, less convenient than surface measurements such as tiltmeter or seismic, and less directly interpretable than coring studies, the microseismic technique provides a combination of resolution, coverage and economy that is difficult to surpass with other methods.

Downhole microseismic monitoring has been applied successfully to hydraulic-stimulation experiments in hot-dry-rock geothermal reservoirs at Fenton Hill, NM[10-12], the U.K.[13,14], Japan[15] and France[16]. Tomography has been performed using these data indicating low-velocity process zones in the seismic region[17]. Additional data processing defined planar features that represent individual joints that slipped[18-20]. These experiments took place in hard, crystalline rock, through which elastic waves propagate efficiently. In spite of poorer wave-propagation properties, stimulation-related microearthquakes have been successfully mapped in sedimentary environments using downhole geophones[21-28]. Production-related microearthquakes have been studied for years[29-32], most work done using surface geophones.

In the following, we will describe remote well microseismic monitoring in the Austin chalk, Giddings field, TX (**Fig. 1**) and the 76 field, Clinton Co., KY (**Fig. 2**). Microearthquakes were associated with hydraulic stimulation in the Austin chalk, and with primary production in Clinton Co. We monitored from existing wells to demonstrate the

economy of the technique. These deployments began as reconnaissance experiments. However, the data were of such quality to allow accurate mapping of the microearthquake data, yielding previously unknown details of the reservoir fracture systems.

Setting

Austin Chalk. The Giddings field was discovered in 1960 by Union Producing Company with the drilling of the Pruess No. 1 well immediately west of the town of Giddings in Lee County, Texas. The field now covers portions of Lee, Burleson, Bastrop, Fayette, Brazos, and Washington Counties. Cumulative production from the Giddings field is over 60 million m^3 (380 million bbl) oil and 60 billion m^3 (2.1 trillion ft^3) gas. In the Giddings field, 98% of the oil has been produced from the Austin chalk.

The Austin chalk is a fractured limestone with a matrix porosity of 10% and matrix permeability of 0.01 to 0.1 millidarcys. The presence of fractures in the Austin chalk at Giddings field is due to the bending of this brittle limestone over a deeper and older Jurassic shelf margin or hinge line, trending NE, roughly parallel to the Gulf coast. Drape of the Austin chalk over this deep seated structure created the fractures which enable the Austin chalk to produce at relatively high rates (160 m^3 or 1000 bbl per day) and reach single well maximum cumulative production approaching 80,000 m^3 (500,000 bbl) of oil. Recovery efficiency for the Austin Chalk at Giddings is thought to be on the order of 7-10% of the original oil in place.

In the Austin chalk, hydraulic stimulation is used to complete new wells and to enhance production from older wells. During stimulation, the water forced into untapped areas of the chalk is thought to replace, and thus mobilize hydrocarbons residing in small cracks through imbibition. To study the stimulated fracture system, we monitored microseismicity during two, 4000 m^3 (25,000 bbl) stimulations of the Austin chalk (peak pressure 21 MPa, 3000 psi; peak flow rate 13 m^3/minute, 80 bbl/minute) that included acid and diverter (rock salt) phases.

Clinton Co. Clinton County is located within the Cumberland Saddle of the Cincinnati Arch, immediately west of the Grenville Front. Oil is produced from low porosity (<2%) carbonate rocks of Ordovician age, spanning the section from the Lexington Limestone to the Knox Group, at depths from 230 to 730 m. Fracture storage and permeability is suggested by isolated, high-volume production wells. Initial production rates as high as 64 m^3 (400 bbl) per hour and cumulative production of 16,000 m^3 (100,000 bbl) from a single well have been reported[33].

Basement-controlled wrench-fault structures have been associated with oil production from shallow (135 to 180 m), carbonate reservoirs, 65 km west of Clinton County[34]. Local operators have also based recent drilling programs on fracture/lineament patterns delineated on side-looking airborne radar images and interpreted to be associated with right-lateral wrenching of an east-west trending basement fault. In general,

only near-vertical fracture sets have been considered in these models. We deployed geophones in Clinton Co. wells to delineate the reservoir fracture systems. Results of two, earlier tests have been presented[35]; here we summarize results of our latest, and most seismically active deployment.

Data

We collected microseismic data using downhole, 3-component geophone tools. A mechanical arm coupled the instruments to the borehole wall. The tools were equipped with 8- or 30-Hz geophones. Downhole amplification of the geophone outputs was 60 dB. At the surface, the data signals were further amplified and anti-alias filtered before input to a digital, PC-based, event-detection system[36]. Data were sampled at 5 KHz. Events from both sites contained clear compressional (P) and shear (S) phases. Shear-to-compressional amplitude ratios were similar to those of tectonic earthquakes, indicating predominantly shear-slip, rather than tensile, source mechanisms.

Austin Chalk. We deployed downhole geophones at two sites in the Giddings field (**Fig. 1**). We monitored from well CPU 1-2 near Cook's Point, depth 2097 m, 9/91 to 11/91, and from wells Matcek 4 and 3 near Caldwell, depths 2259 m and 2280 m, 11/91 to 9/92 and 5/92 to 9/92, respectively. Wells were prepared by removing production tubing, setting temporary bridge plugs just above the perforated interval and filling with non-corrosive fluid.

Over 480 and 770 microearthquakes were collected during stimulations of wells CPU 2-2 and Matcek 1, respectively. At both sites, seismicity started within one hour of the pumping and decayed away after final shut-in (**Fig. 3**). Signal energy peaked between 200 and 500 Hz (**Fig. 4**). Horizontally polarized S waves arrived earlier than vertically polarized S waves, suggesting bedding-related anisotropy. This effect required us to rotate horizontal-component seismograms to radial and transverse to consistently determine S-wave arrival times. Rotation was based on P-wave particle motion (referred to as the hodogram in this manuscript) which should lie entirely on the radial component. S-wave reflections off the high-contrast Eagleford-Buda boundary below the Austin chalk arrive after the direct S waves in many records. These reflections became important for determining event depths. Perforation shots fired at both injection points produced good-quality records and helped to calibrate velocities and geophone orientations.

Clinton Co. We deployed two geophones in well GT8 at depths of 427 and 244 m, 1/95 to 8/95. A third geophone was placed in well BU1 at a depth of 396 m, 3/95 to 8/95 (**Fig. 2**).

Monitoring began 6 weeks after initial production from well HT1 (**Fig. 5**). The production-rate decrease at week 13 was followed by an event-rate decrease at week 15. We presume production declined after week 22, but records were not available. Production ceased in week 28 before the well was deepened. Monitoring was off line for weeks 29 to 30 and only two events were detected between weeks 31 and 36.

We recorded over 3200 events, average rate 20 events per day over the first 23 weeks. Records contained energy between 100 and 700 Hz (**Fig. 6**). Slight anisotropy was observed, horizontally-polarized S waves usually arriving early. Reflections were also observed but were not used to locate microearthquakes because data from the two geophones in well GT8 constrained depths well. Three shots were recorded for calibration purposes.

Calibration and Location Methods

Deployments consisted of three or fewer downhole stations, which required us to use a combination of P- and S-wave arrival times and P-wave hodogram azimuths to obtain locations. Arrival times were determined manually. Eigenvector analysis[37] was used to compute hodogram azimuths using the first half-cycle of the horizontal-component P wave. These data gave the propagation azimuth of the P wave, used to constrain the event location.

Calibration of the field site consisted of estimating seismic velocities, station time corrections and azimuthal geophone orientations. Depths to major geological interfaces were taken from well log data, most often resistivity. All sites were well approximated by horizontally layered structural models. Initial P-wave velocity was taken from well logs and perforation shot data. S-to-P velocity ratios could also be obtained from perforation shots, but were unreliable because perforation shot records contained poor S waves. Perforation shot hodograms gave initial estimates of geophone orientation.

The velocity and orientation estimates were refined using a joint-hypocenter-velocity inversion, performed using a subset of events with high-quality, arrival-time and hodogram data. The inversion adjusted unknown velocities, station time corrections, geophone orientations and event locations to fit the arrival-time and hodogram data in a least-squares sense. Units were scaled so timing and angular data were of similar magnitude. Data were weighted by estimates of uncertainty. The parameter separation technique[38] was used so an unlimited number of events could be included. Once a site was calibrated, the remaining event locations could be calculated using standard techniques, employing similar scaling and weighting as above.

Results

Austin Chalk. Initial attempts at locating Austin chalk microearthquakes using hodogram inclinations to constrain depths fared poorly (**Fig. 7**). Events fell well beneath the producing zone, in the more ductile, Eagleford shale. Because the results were so unrealistic, we decided to include reflected phases in the analysis.

Calibration was performed using 90 high-quality events containing two P and two S arrivals and at least one reflected arrival recorded by the two-geophone array during stimulation of the Matcek 1. Results gave a P velocity of 4.71 km/s for the Austin chalk, matching the sonic-log value from a well near Cook's Point. S velocity was 2.38 km/s. The S velocity in the Eagleford shale, beneath the Austin chalk, was constrained by the reflected phase to 1.80 km/s.

Depths of the 90, high-quality microearthquakes were constrained very well by the reflection data, (**Fig. 8**). Most events fell within 20 m of the base of the Austin chalk. We also located Cook's Point events that had all three P, S and reflected phases using the velocities obtained above. Depths were not as well constrained, but still clustered around the base of the Austin chalk.

Given the narrow depth range of the high-quality events, we fixed event depth to the middle of the production interval near the base of the Austin chalk. This allowed the location of over 240 Matcek-1 stimulation events, defining a linear trend parallel to the expected fracture trend in the Giddings (**Fig. 9**). The most distant events were over 700 m from the Matcek-3 geophone. The entire wing of the stimulation was visible, although the density of locatable events decreased near the injection point. The seismic zone was less than 30 m wide over much of its length.

For the single-station experiment at Cook's Point, all locations were based on P and S (vertically polarized) arrival times and a hodogram azimuth. P waves strong enough to provide high-quality azimuths occurred for only 96 events. We obtained two groups of locations, symmetrical about the station position, because of the ambiguity in hodogram direction. The most likely group aligned with the stimulation well in the direction expected from regional geology (**Fig. 9**). The most distant locatable events were just over 400 m from the monitor station. Thus, we saw only a portion of one wing of the stimulation. The width of the seismic zone was 150 m over most of the observable length. The width was constrained well by P and S arrival times and was affected little by hodogram error.

Clinton Co. We calibrated the site using events with three P and three S arrival times, and at least two hodogram azimuths. Setting a layer boundary at the top of the High Bridge (344 m), we obtained P velocities of 5.86 and 6.31 km/s and S velocities of 3.09 and 3.23 km/s. Estimates of geophone orientations were adjusted up to 5° from the initial, perforation-shot estimates. The refined geophone orientations were important in aligning locations of events collected before and after deployment of the third geophone. After calibration, we located over 1700 events (**Fig. 10**). Three fracture planes strike N65°E and dip 15° to 20° to the NW or to the SE. The deepest fracture (group C in **Fig. 10**) was difficult to see, but stood out because of its unique, S-nodal (large P, small S) waveforms on the upper GT8 geophone. This plane contained over 200 events forming an elongate planar pattern that intersected the main fracture (group B) along its northern, well-defined edge. Composite focal mechanisms have indicated nearly pure reverse faulting along these fractures[39].

Discussion

We collected over 480 and 770 microearthquake events at two Austin chalk sites in the Giddings field, 20% and 31% could be located, respectively. In Clinton Co. we collected over 3200 events, locating 53%. We were encouraged by such successful

studies, given the restriction of deploying geophones only in existing wells.

In the Austin chalk, production tubing had to be pulled from wells prior to monitoring. Geophone tools that can be deployed in production tubing or in the annulus will cut this expense from future studies.

Because hodogram inclinations could not be relied on (**Fig. 7**), locating Austin chalk events depended on the use of reflected phases to constrain depths (**Figs. 4, 8**). However, high-quality reflections were present in a minority of events. In Clinton Co. we placed two geophones in one well, 180 m apart, providing depth control for nearly all events.

Austin Chalk. If Austin chalk shear-slip events resulted from elevated pore pressure during hydraulic stimulation, the seismic zone should be comparable to the region of the reservoir that was subject to imbibition, or the replacement of hydrocarbons in microcracks with water by capillary action.

Both Austin chalk seismic zones were similarly oriented, parallel to the trend of the regional folding responsible for the reservoir fracture system. However, the Cook's Point seismic zone was five times wider than the Matcek zone. Perhaps a more dense fracture network enabled stimulation over a wide zone at Cook's point, while more competent rock caused the stimulation to drive a single fracture over a long distance at the Matcek site. Production records show a large increase in oil rate from the Cook's Point well immediately following stimulation, but little increase from the Matcek well (**Fig. 11**). The production records suggest that the microseismic patterns are directly related to the effectiveness of the stimulation.

The microearthquake locations fell into a narrow depth interval during the Matcek stimulation (**Fig. 8**). Reservoir engineers predicted containment of the stimulation between a thin, ductile, volcanic ash layer within the Austin chalk and the Eagleford shale. Microearthquake locations supported the containment prediction at the Matcek site.

Clinton Co. Clinton Co. microearthquakes defined three, low-angle, reverse slip, fracture zones (**Fig. 10**). Seismic activity was clearly related to the production of over 1300 m^3 (8100 bbl) of oil from well HT1 (**Fig. 5**). However, the seismically active fractures fell above and below the HT1 production interval. The mapped fractures intersected, or could be extrapolated to old production intervals in wells GT1, GT2 and GT4. A cumulative volume of 725 m^3 (4600 bbl) of oil was extracted from these three wells in the 9 months preceding monitoring. Well GT10 was drilled into the main mapped fracture (Group B in **Fig. 10**), and produced brine. Later, well HT1 was deepened, encountering brine within 3 m of the same mapped fracture. Therefore, the microearthquakes defined previously drained, oil-bearing fractures that subsequently filled with brine, presumably resulting from an active, but poorly connected water drive[39].

The observed relation between seismic activity and production is predicted by poroelastic models[30]. We expect no seismicity on the draining fracture because pore pressure was reduced, allowing stress normal to the fault surface to increase, thus inhibiting slip. The model predicts small increases in horizontal compression above and below the drained fracture.

In the horizontal-compression stress regime indicated by focal mechanism results[39], the additional stress could have triggered slip on fractures that were already stressed to near failure.

Density and/or temperature logging data show anomalies 1 to 2 m thick in wells that intersect the seismically active fractures. Porosity estimates fell between 15% and 35%. Taking a 300 by 90 by 1 m zone of 15% porosity gives 4050 m^3 (25000 bbl) storage capacity.

The presence of low-angle, oil-bearing fractures has implications for field development. Drilling horizontal or deviated wells does not increase the probability of intersecting productive fractures. Dip meter and formation micro-scanning logs may be very useful in determining orientations of low-angle, productive fractures and thereby aid in more effective placement of offset wells. Interwell correlation and mapping of the conductive fractures will allow better planning in plug-and-abandonment operations so as to avoid premature contamination of pay zones with water. Pressure maintenance operations could also be attempted once the conductive fracture zones between wells have been mapped.

Conclusions

1. Over 480 and 770 stimulation-induced microearthquakes were recorded at two sites in the Austin chalk, Giddings field, TX and over 3200 production-induced microearthquakes were recorded at Clinton Co., KY, deploying geophones in existing boreholes.

2. Hodogram-inclination data caused Austin chalk events to locate out of zone, leading to the use of reflected phases for depth control. In Clinton Co., dual geophone deployment in a single well constrained event depths successfully.

3. Combining shot and well log data with a joint hypocenter-velocity inversion allowed us to calibrate seismic velocities and downhole geophone orientations and to calculate accurate microearthquake locations. Of those collected, 20% and 31% of Austin chalk and 53% of Clinton Co. microearthquakes could be located.

4. At two Austin chalk sites, microearthquake patterns indicated different stimulation-zone widths; the wider zone yielded higher post-stimulation production. Reflected phases constrained microearthquake depths which fell within the lower, stimulated zone of the Austin chalk.

5. At Clinton Co., microearthquakes defined previously drained, high-porosity, low-angle, reverse slip, fracture zones that are currently filled with brine. No seismicity intersected the producing interval. These observations are consistent with poroelastic models[30].

References

1. Snaman, D.K., Hunter, R.J. and Wood, M.D., "Tiltmeter mapping of fractures in granitic rock at Wawona, Yosemite National Park, California," *EOS Trans, Am. Geophys. Union*, (1993) **74**, 582.

2. Barton, C.A., Zoback, M.D. and Moos, D., "Fluid flow along potentially active faults in crystalline rock," *Geology*, (1995) **23**, 683.

3. Stewart, R. R., R. M. Turpening and M. N. Toksoz, "Study of a subsurface fracture zone by vertical seismic profiling," *Geophys. Res. Lett.*, (1981) **8**, 1132.

4. Turpening, R. M. and C. Blackway, "Differential vertical seismic profiling: The hydrofrac," in Balch, A., and Lee, M., Eds., *Vertical Seismic Profiling*, Internat. Human Res. Develop, Corp., (1984).

5. Niitsuma, H. and H. Saito, "Evaluation of the three-dimensional configuration of a subsurface artificial fracture by the triaxial shear shadow method", *Geophysics*, (1991) **56**, 2118.

6. Meadows, M. A. and D. F. Winterstein, "Seismic detection of a hydraulic fracture from shear-wave VSP data at Lost Hills Field, California", *Geophysics*, (1994) **59**, 11.

7. Warpinski, N. R. and L. W. Teufel, "Influence of geologic discontinuities on hydraulic fracture propagation," *JPT*, (1987) **39**, 209.

8. Fast, R. E., Murer, A. S. and Timmer, R. S., "Description and analysis of cored hydraulic fractures, Lost Hills Field, Kern County, California," presented at the 1992 SPE Annual Technical Conference and Exhibition.

9. Mueller, M. C., "Using shear waves to predict lateral variability in vertical fracture intensity," *The Leading Edge*, (1992) **11**, 29.

10. Pearson, C., "The relationship between microseismicity and high pore pressure during hydraulic stimulation experiments in low permeability granite rocks," *J. Geophys. Res.* (1981) **86**, 7855.

11. Albright, J. N. and C. F. Pearson, "Acoustic emissions as a tool for hydraulic fracture location: experience at Fenton Hill Hot Dry Rock site," *SPE Journal* (1982) **22**, 523.

12. House, L. S., "Locating microearthquakes induced by hydraulic fracturing in crystalline rock," *Geophys. Res. Lett.*, (1987) **14**, 919.

13. Batchelor, A. S., R. Baria and K. Hearn, "Monitoring the effects of hydraulic stimulation by microseismic event location, a case study," paper SPE 12109, presented at the 1983 SPE Annual Technical Conference and Exhibition, San Francisco, October 5-8.

14. Baria, R. and A. Green, "Seismicity induced during a viscous stimulation at the Camborne School of Mines Hot Dry Rock geothermal Energy project in Cornwall, England," *Proc. Progress in Acoustic Emission*, (1986) **3**, 407.

15. Niitsuma, H., N. Chubachi and M. Takanohashi, "Acoustic emission analysis of a geothermal reservoir and its application to reservoir control," *Geothermics,* (1987) **16**, 47.

16. Cornet, F. H., "Projet Mayet de Montagne, Etude in situ de la percolation forcee d'eau an milieu granitique" (in French), *Final Report, IPGP*, (Sept. 1988).

17. Block, L., M. C. Fehler, C. H. Cheng and W. S. Phillips, "Seismic imaging using microearthquakes induced by hydraulic fracturing," *Geophysics*, (1994) **59**, 102.

18. Fehler, M.C., Houxe, L.S. and Kaieda, H., "Determining planes along which earthquakes occur: method and application to earthquakes accompanying hydraulic fracturing," *J. Geophys. Res.*, (1987) **92**, 9407.

19. Roff, A., Phillips, W.S. and D.W. Brown, "Joint structures determined by clustering microearthquakes using waveform amplitude ratios", *Int. J. Rock Mech. Geomech. Abs.*, in press.

20. Phillips, W.S., House, L.S. and Fehler, M.C., "Detailed joint structure in a geothermal reservoir from studies of induced microearthquake clusters", submitted to *J. Geophys. Res.*

21. Dobecki, T. L., "Hydraulic fracture orientation by use of passive borehole seismics," paper SPE 12110, presented at the 1983 SPE Annual Technical Conference and Exhibition, San Francisco, October 5-8.

22. Sarda, J.-P., P. J. Perreau and J.-P. Deflandre, "Acoustic emission interpretation for estimating hydraulic fracture extent," paper SPE 17723, presented at the 1988 SPE Gas Technology Symposium, Dallas, June 13-15.

23. Fix, J., R. Adair, T. Fisher, K. Mahrer, C. Mulcahy, B. Myers, J. Swanson, J. Woerpel, "Development of microseismic methods to determine hydraulic fracture dimensions," *Gas Res. Inst., Tech. Rep.* (1989) **No. 89-0116**.

24. Vinegar, H. J., P. B. Wills, D. C. DeMartini, J. Shylapobersky, W. F. Deeg, R. G. Adair, J. C. Woerpel, J. E. Fix and G. G. Sorrells, "Active and passive seismic imaging of a hydraulic fracture in diatomite," paper SPE 22756, presented at the 1991 SPE Annual Technical Conference and Exhibition, Dallas, Texas, October 6-9.

25. Stewart, L., B. R. Cassell and G. M. Bol, "Acoustic-emission monitoring during hydraulic fracturing," *SPE Formation Evaluation* (1992) **7**, 139.

26. Keck, R.G. and Withers, R.J., "A field demonstration of hydraulic fracturing for solid waste injection with real-time passive seismic monitoring," paper SPE 28495, presented at the 1994 SPE Annual Technical Conference and Exhibition, New Orleans.

27. Zhu, X., Gibson, J., Ravindran, N., Zinno, R., Sixta, D., "Seismic imaging of hydraulic fractures in Carthage tight sands: A pilot study," *The Leading Edge*, (1996) **15**, 218-224.

28. Warpinski, N.R., Engler, B.P., Young, C.J., Peterson, R., Branagan, P.T. and Fix, J.E., "Microseismic mapping of hydraulic fractures using multi-level wireline receivers", paper SPE 30507, presented at the 1995 SPE Annual Technical Conference and Exhibition, Dallas.

29. Pennington, W.D., S.D. Davis, S.M. Carlson, J. Dupree, and T.E. Ewing, "The evolution of seismic barriers and asperities caused by the depressuring of fault planes in oil and gas fields of South Texas," *Bull. Seism. Soc. Am.*, (1986) **76**, 939.

30. Segall, P., "Earthquakes triggered by fluid extraction," *Geology*, (1989) **17**, 942.

31. Grasso, J.R., and G. Wittlinger, "Ten years of seismic monitoring over a gas field," *Bull. Seism. Soc. Am.*, (1990) **80**, 450.

32. Doser, D.I., M.R. Baker, and D.B. Mason, "Seismicity in the War-Wink gas field, Delaware Basin, Texas, and its relationship to petroleum production," *Bull. Seism. Soc. Am.*, (1991) **81**, 971.

33. Hamilton-Smith, T., B.C. Nuttall, P.J. Gooding, D. Walker, and J.A. Drahovzal, "High-volume oil discovery in Clinton County, Kentucky," *Kentucky Geological Survey, Series 11, Information Circular 33*, (1990).

34. Black, D.F.B., "Oil in dolomitized limestone reservoirs in Kentucky, *Proc. 6th Int. Conf. Basement Tectonics*, (1986) 140.

35. Rutledge, J.T., Phillips, W.S., Roff, A. Albright, J.N., Hamilton-Smith, T., Jones, S.K. and Kimmich, K.C., "Subsurface fracture mapping using microearthquakes detected during primary oil production, Clinton County, Kentucky", paper SPE 28384,

presented at the 1994 SPE Annual Technical Conference and Exhibition.

36. Lee, W.H.K., "Tookbox for seismic data acquisition, processing and analysis," *IASPEI Software Library*, (1989) **1**.

37. Flinn, E. A., "Signal analysis using rectilinearity and direction of particle motion", *Proc. IEEE*, (1965) **53**, 1725.

38. Pavlis, G.L. and Booker, J.R., "The mixed discrete-continuous inverse problem: Application to the simultaneous determination of earthquake hypocenters and velocity structure," *J. Geophys. Res.*, (1980) **85**, 4801.

39. Rutledge, J.T., Phillips, W.S. and Schuessler, B.K., "Reservoir characterization using oil-production induced microseismicity, Clinton County, Kentucky, " *Tectonophysics*, in press.

Cook's Point

CPU 1-2
(geophone)

CPU 2-2
(injection)

0 2000
Feet

Matcek Ranch

M3 (geophone)

6H

M1
(injection)

M4 (geophone)

0 2000
Feet
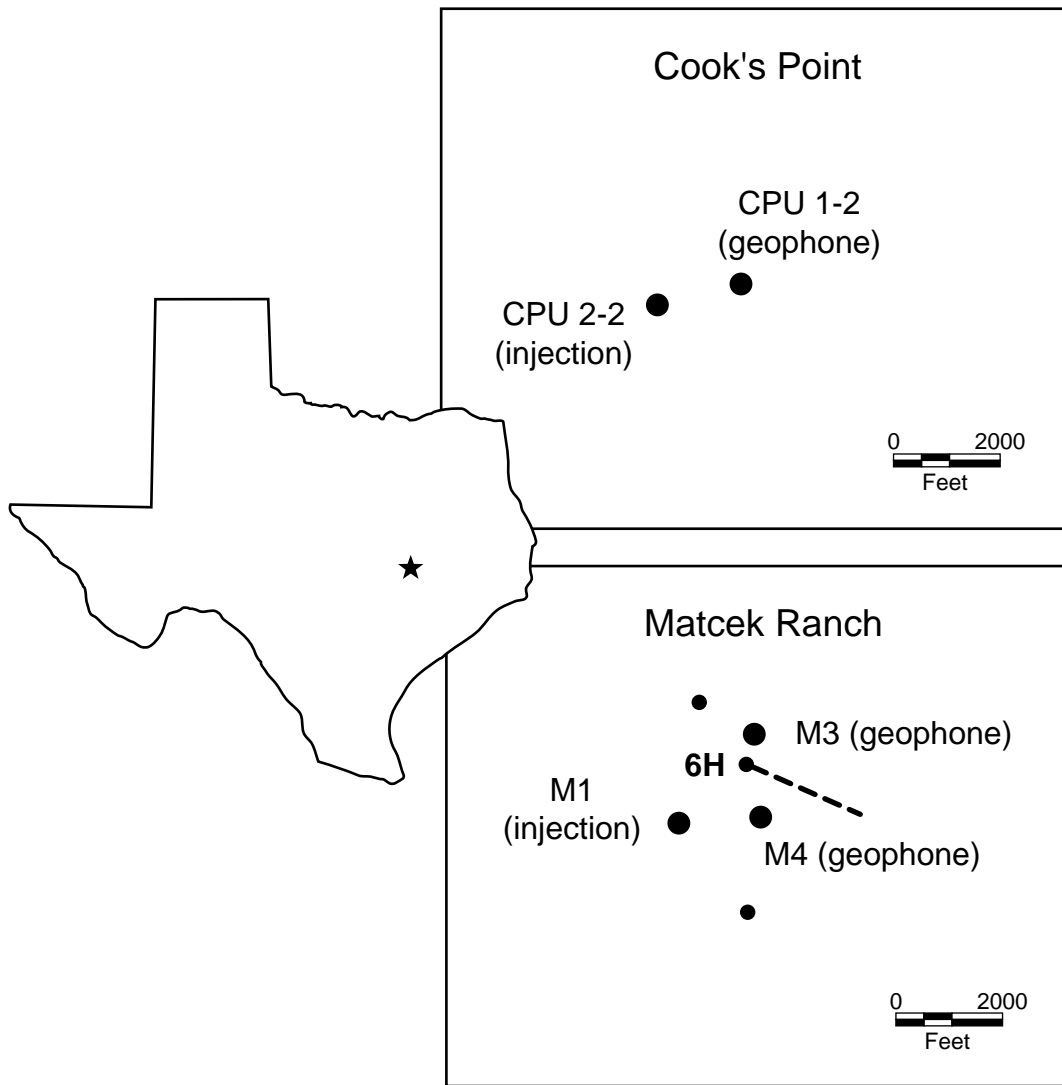
Figure 1. Map of monitoring sites in the Giddings field, TX.
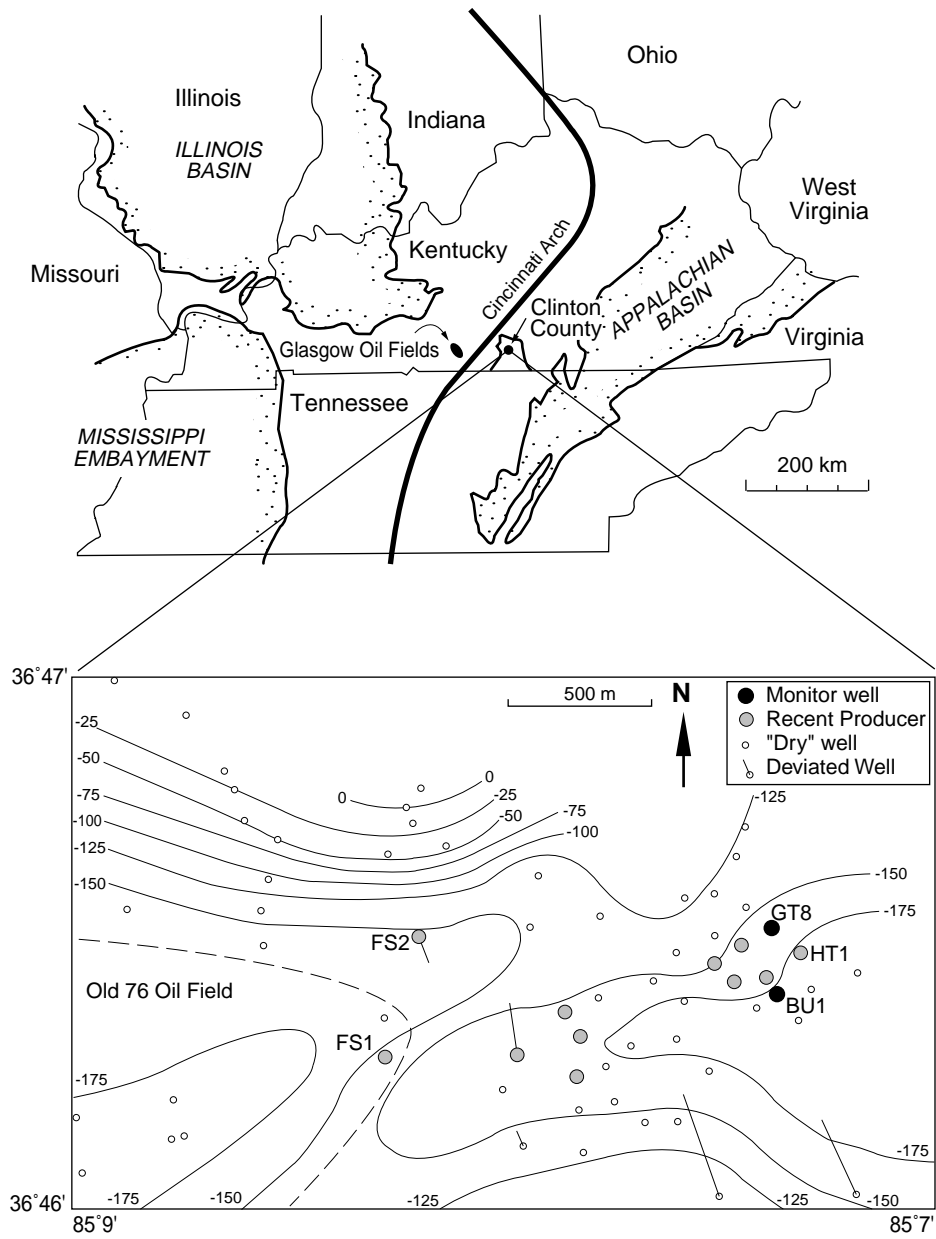
Figure 2. Map of monitoring site in Clinton Co., KY.
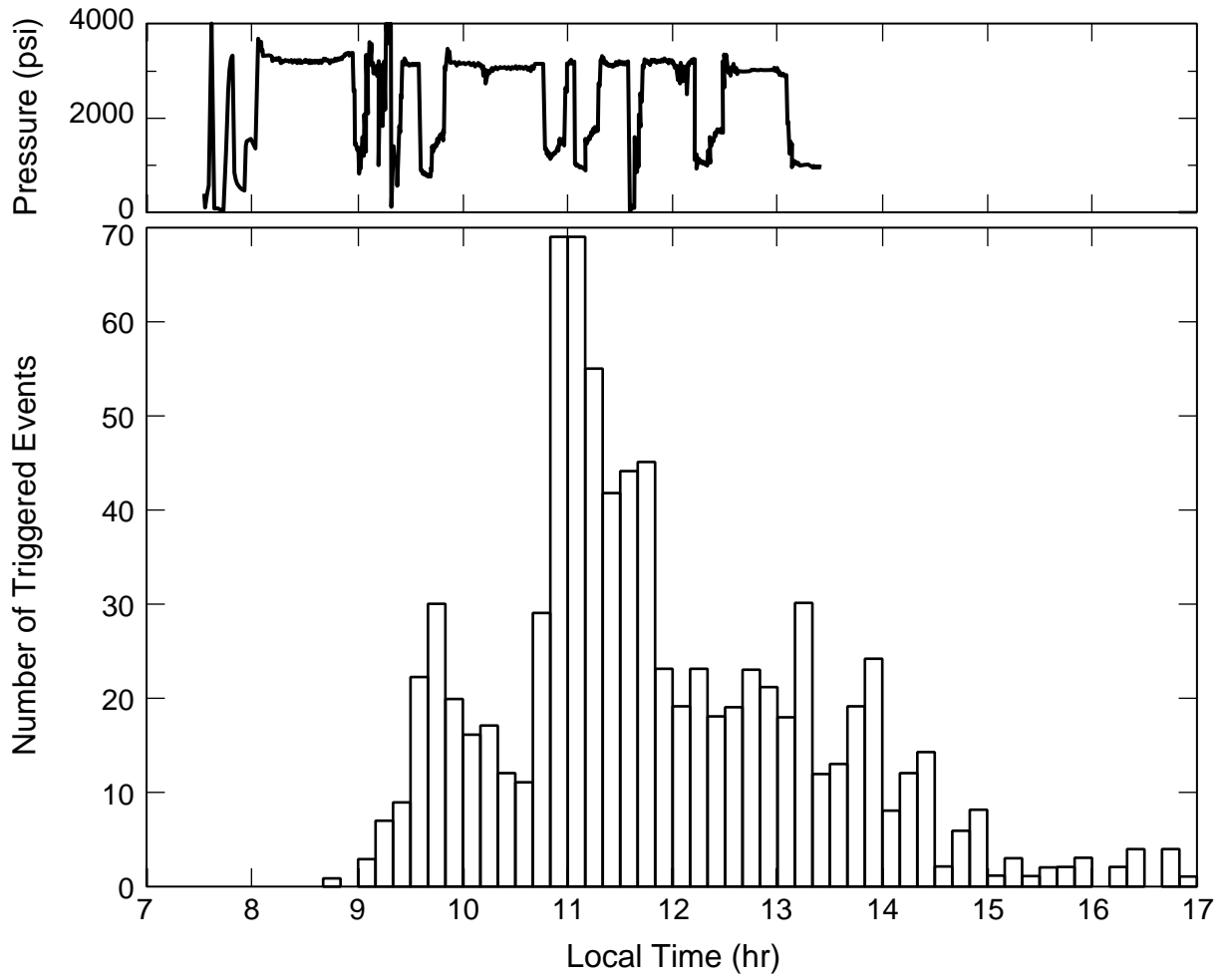
Figure 3. Event histogram and well-head pressure during hydraulic stimulation, well CPU2-2, Giddings field, TX.
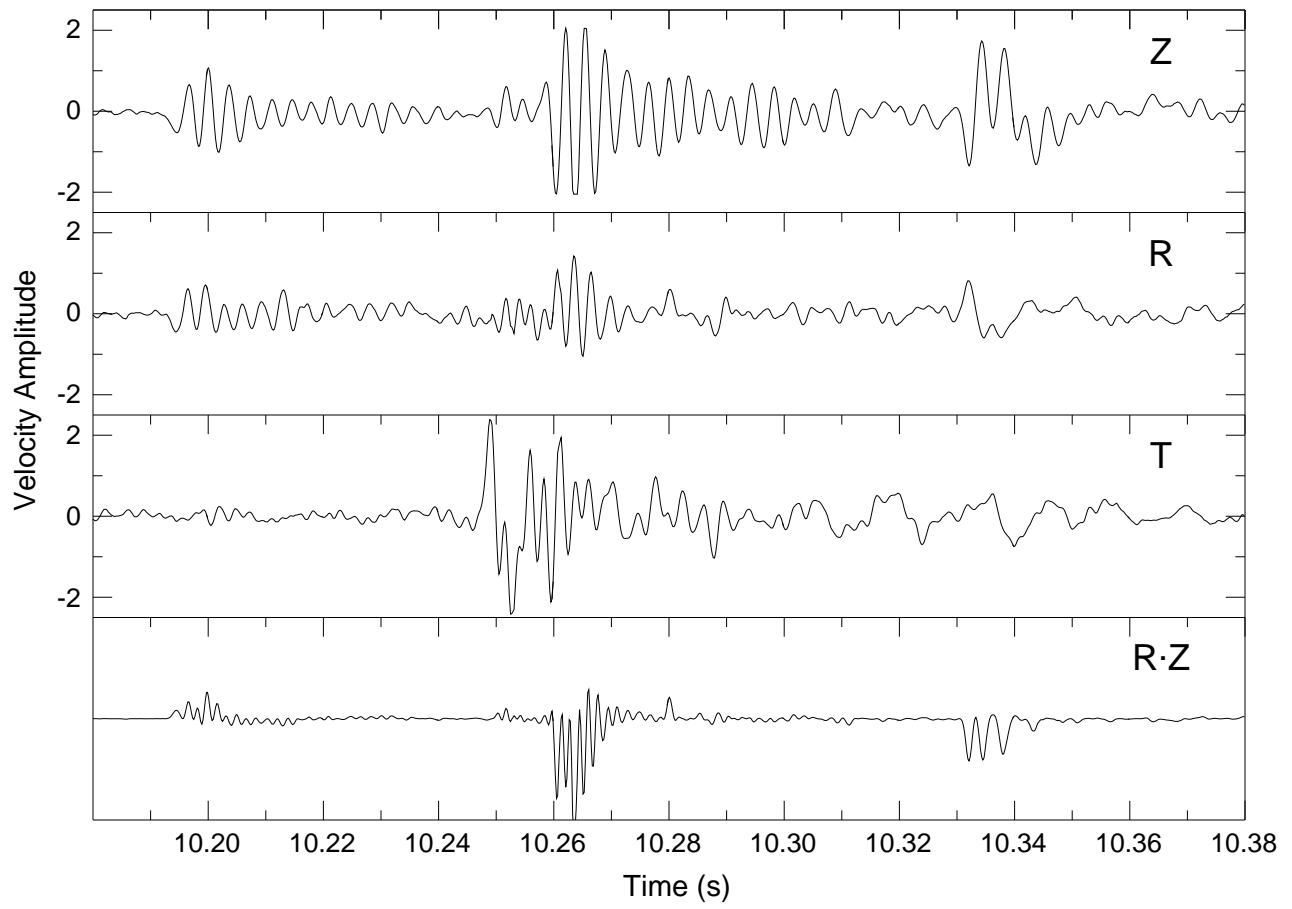
**Figure 4. Vertical, radial, transverse and radial-vertical product traces, CPU2-2 stimulation, Giddings field, TX.**
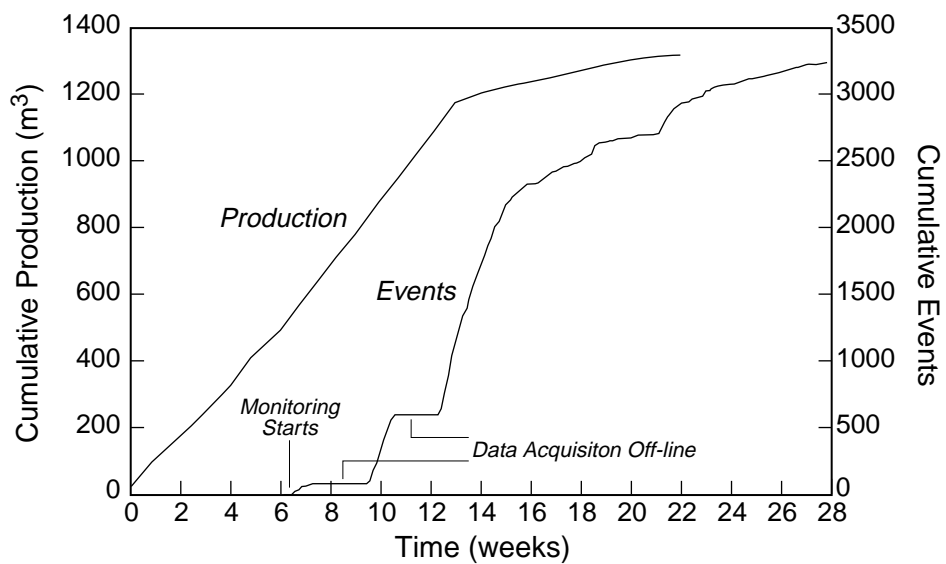
Figure 5. Cumulative production, well HT1 and cumulative number of events, Clinton Co., KY.
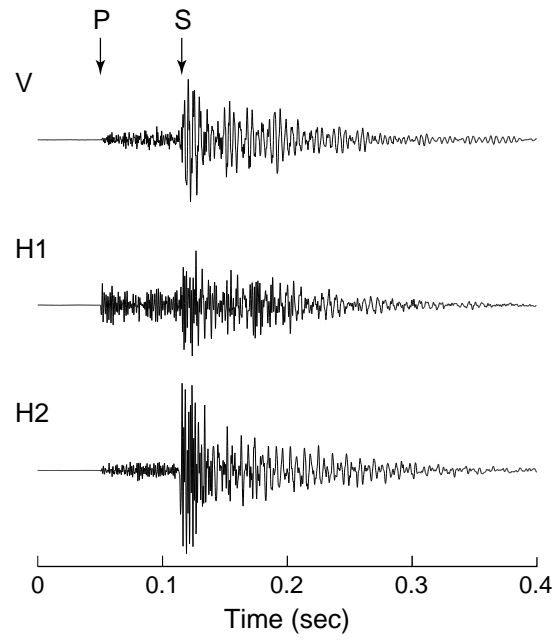
Figure 6. Vertical, upper- and lower-horizontal (unrotated) seismograms, Clinton Co., KY.
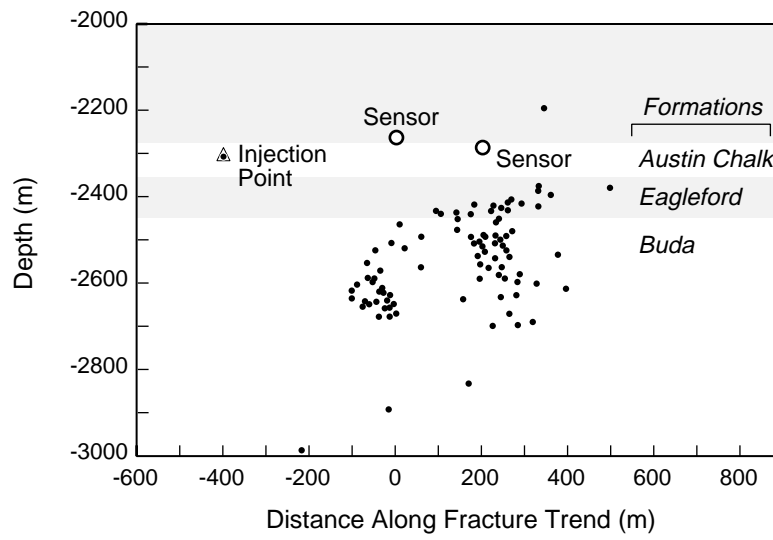
Figure 7. Locations calculated using hodogram inclinations, CPU2-2 stimulation, Giddings field, TX.
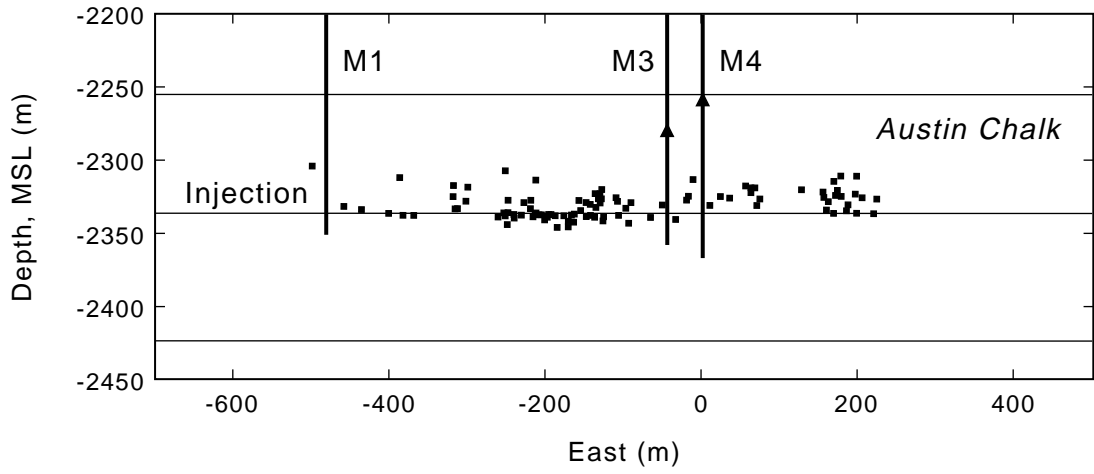
Figure 8. locations calculated using reflected phases, Matcek 1 stimulations, Giddings field, TX.
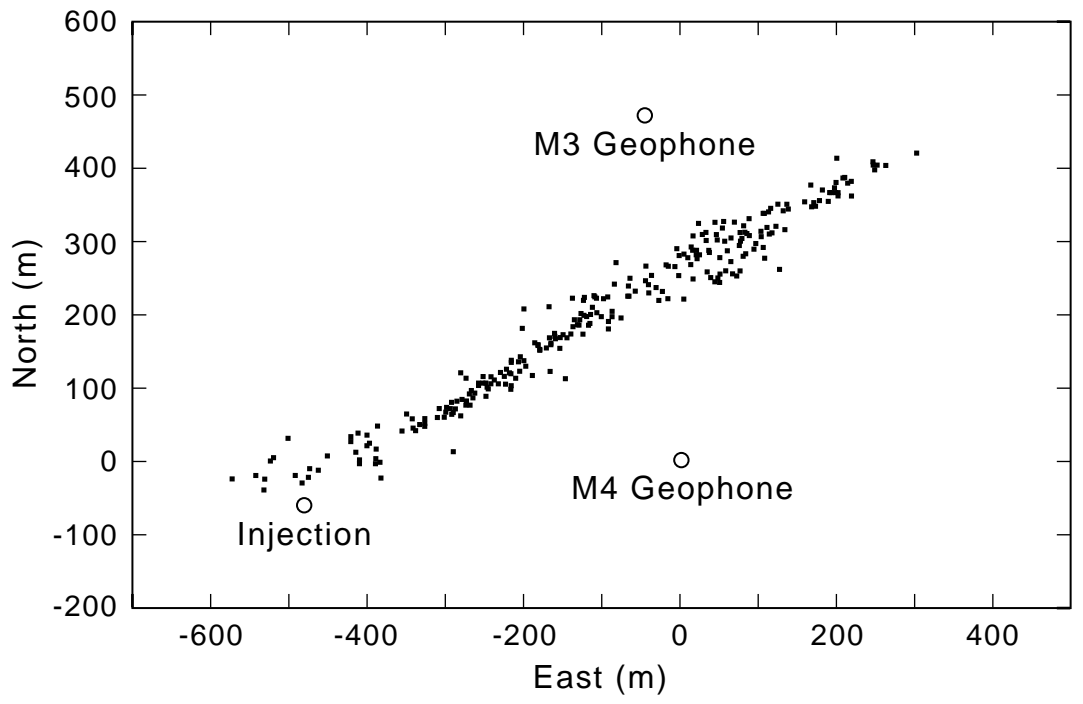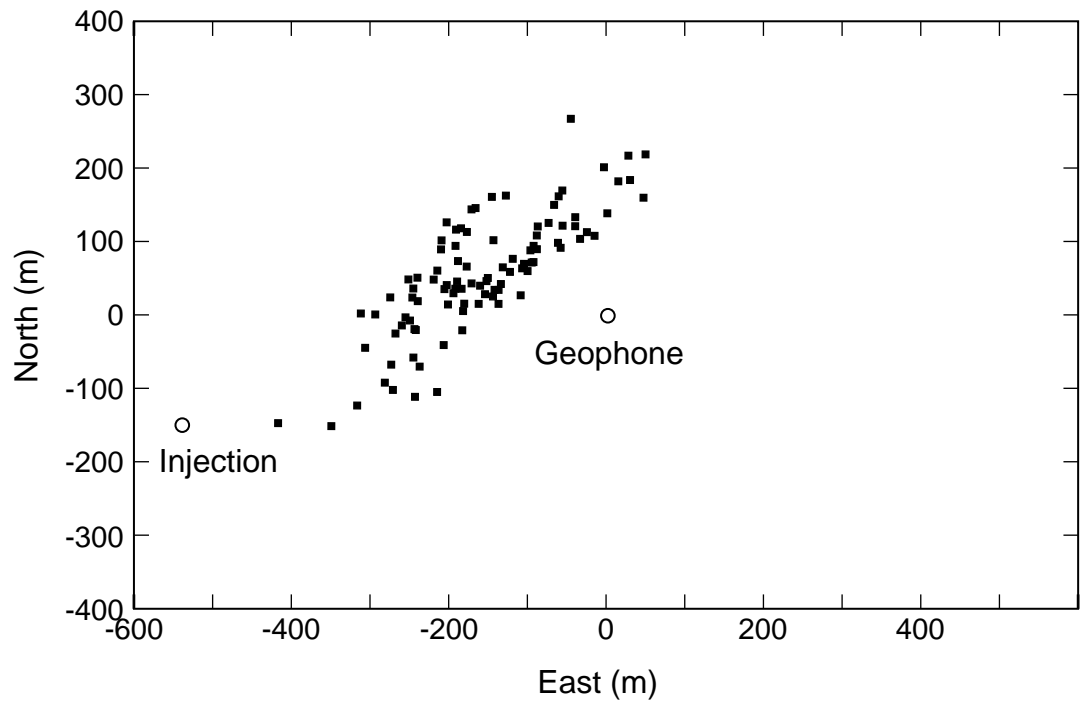
Figure 9. Map view locations, CPU2-2 and Matcek 1 stimulations, Giddings field, TX.
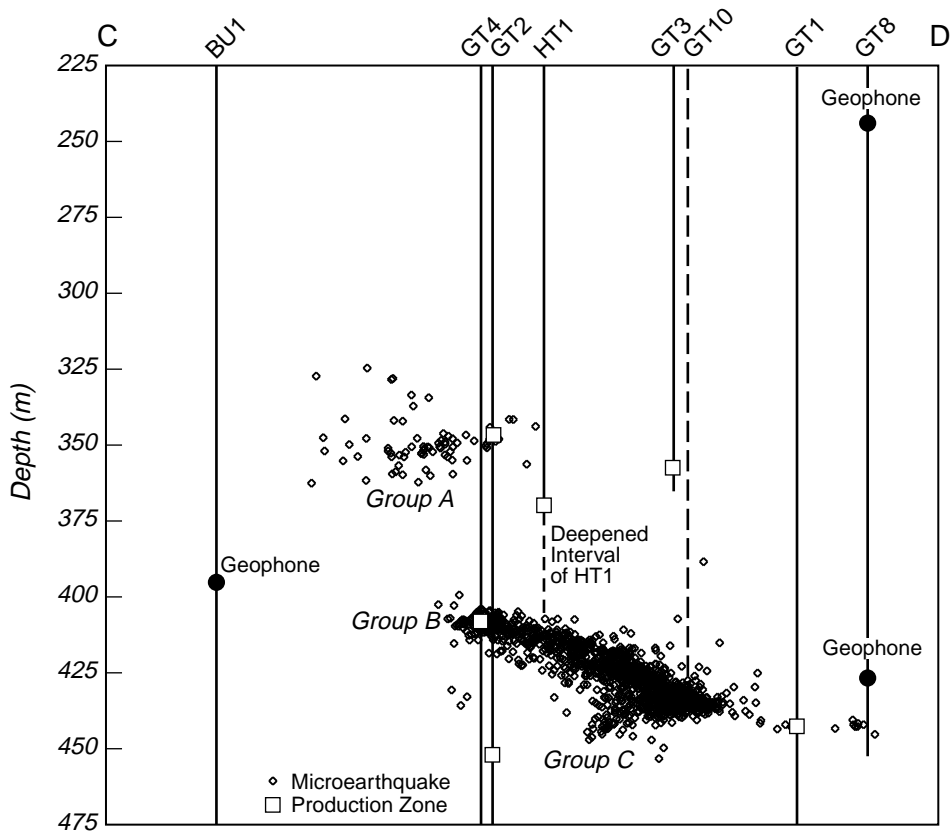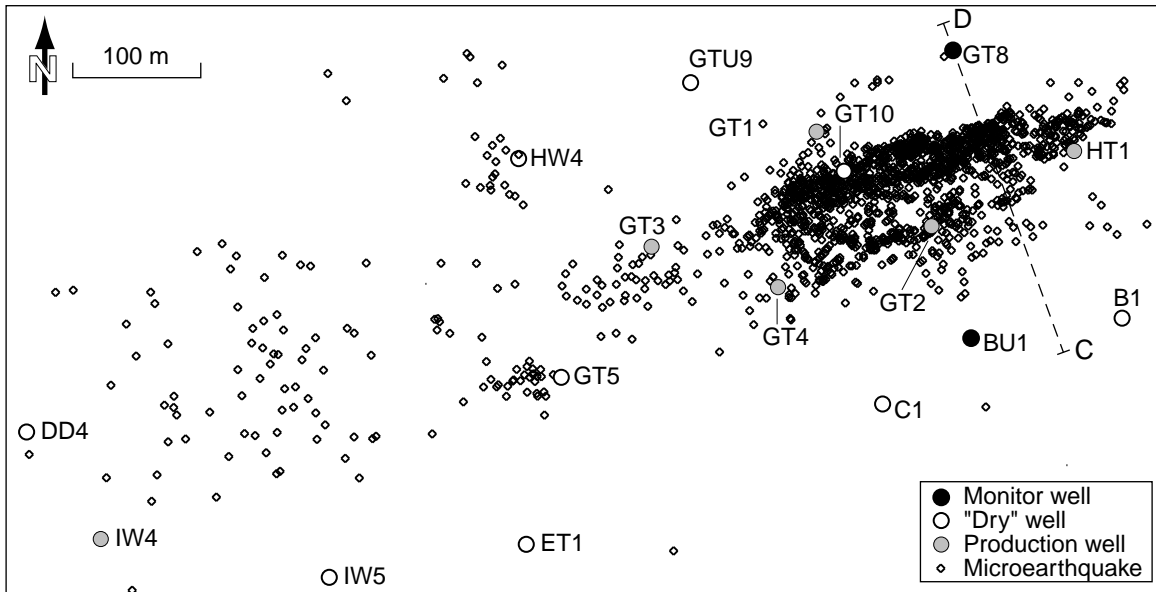
**Figure 10. Map and cross-section view locations, Clinton. Co., KY.**
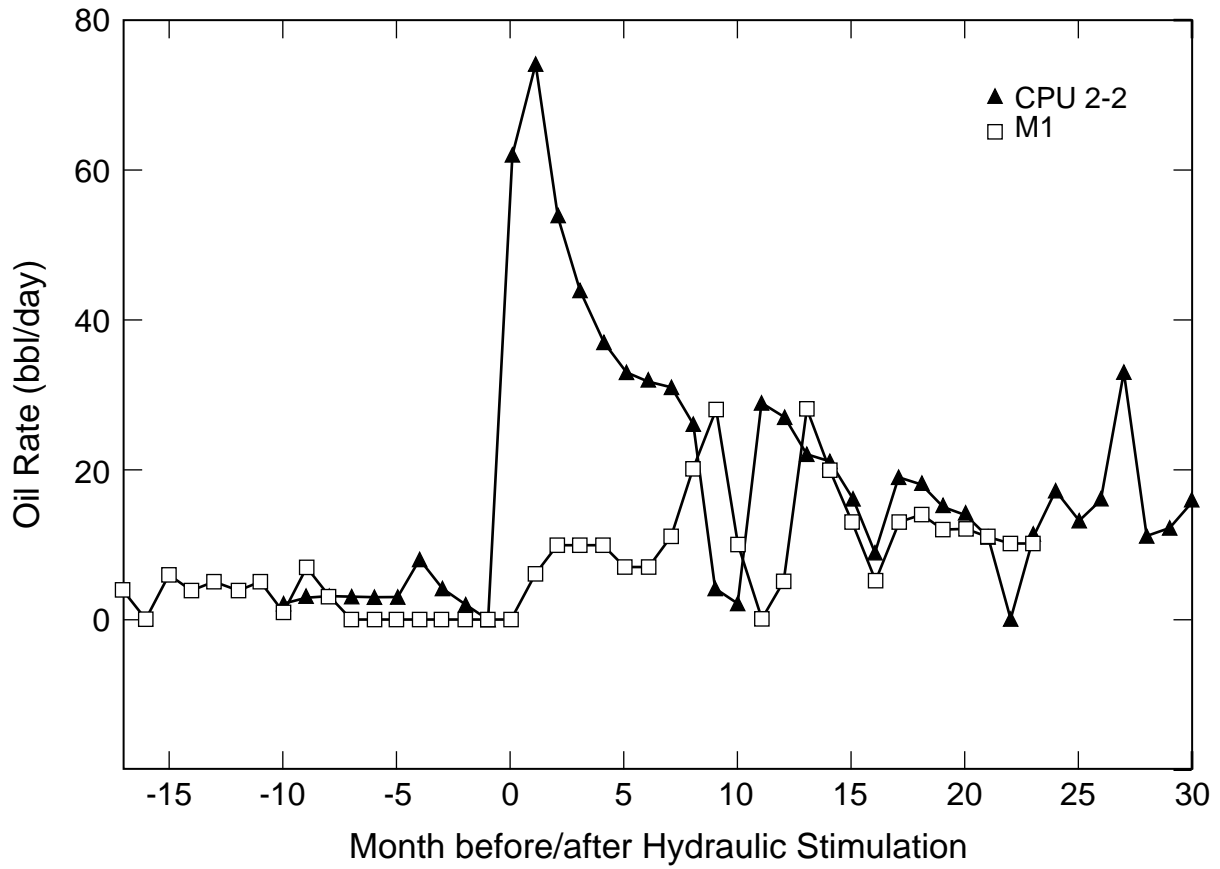
Figure 11. Pre- and post-stimulation production, CPU2-2 and Matcek m1 wells, Giddings field, TX.